Journal of Applied Fluid Mechanics, Vol. 16, N9. x, pp. 1877-1886, 2023.
Available online at www.jafmonline.net, ISSN 1735-3572, EISSN 1735-3645.
https://doi.org/10.47176/jafm.16.09.1626

Leading Edge Radius Effects on VAWT Performance

N. Davandeh and M. J. Maghrebi†

Mechanical Engineering Department, Ferdowsi University of Mashhad, Mashhad, Iran

†*Corresponding Author Email: mjmaghrebi@um.ac.ir*

ABSTRACT

Numerous studies have been conducted to investigate effect of blade geometry of vertical axis wind turbine performance. Most of the evaluations have focused on the airfoil series and airfoil geometry parameters such as thickness and camber of the airfoil. Few studies have examined the effect of other blade geometry parameters on the vertical axis wind turbine performance. In the present study, the effect of geometric change in leading-edge radius (LER) of a vertical axis wind turbine performance has been numerically studied. Hence, modified NACA 0021 airfoil profiles were created using the geometric method (CST). Then, the flow behavior around a Darrieus vertical axis wind turbine was simulated under the influence of the reduction and set-up coefficients of the leading-edge radius at a constant wind speed of 9 m/s and a tip speed ratio of 1.5 to 3.5 using the computational fluid dynamics. Additionally, the effects of the examined parameter (leading-edge radius) on fluid flow and aerodynamic performance coefficients, including the coefficients of power and torque, were investigated. The results indicated that the leading-edge radius affected the near wake flow of the turbine, and the optimization of leading-edge radius parameter controls the dynamic stall and reduces the formation of a vortex. Finally, the optimization of LER revealed that at 20% reduction in the LER the performance of the turbine at tip speed ratio of 1.5 was increased by more than 50%. This reinforces the self-starting capability of a Darrieus wind turbine.

Article History

Received October 18, 2022
Revised May 17, 2023
Accepted May 17, 2023
Available online July 1, 2023

Keywords:

Darrieus wind turbine
Computational Fluid Dynamics (CFD)
Class functions/Shape functions Transformation (CST)
Dynamic stall
Leading-Edge Radius (LER)

1- INTRODUCTION

Darrieus wind turbine with straight blades is a lift-based vertical axis wind turbine, which can be used in urban areas and regions with complex unsteady flow owing to its features such as no dependence on wind direction, the ability to operate in low altitude areas, and low aerodynamic noise generation (Taban et al., 2020). Although the use of the Darrieus wind turbine has many advantages, the application of this type of turbine has limitations. The aerodynamic characteristics of Darrieus vertical axis wind turbines are complex. In some cases, this type of turbine has self-starting problems when it starts working. Furthermore, its maximum performance is prevented by the phenomena resulting from transient aerodynamic (Ragheb, 2008; Lee & Jang, 2016; Shahizare et al., 2016).

Dynamic stall is one of the problems in designing vertical-axis wind turbines (Karbasian et al., 2022). *Dynamic stall* is an aerodynamic, transient, and non-linear phenomenon leading to a drop in lift and strong fluctuations of the turbine blades. Several parameters affect the dynamic stall; however, due to the low angular velocity of rotor rotation, the influential factors in a vertical axis wind turbine can be limited to only a few crucial factors. The factors that have attracted researchers' attention thus far include airfoil geometry, Reynolds number (Ouro et al., 2018), and angle of attack (AOA) (Sagharichi et al., 2017). The use of the control mechanism of the angle of attack (the wind flow angle with an airfoil) and/or an increase in the Reynolds number (the ratio of inertial force to viscous force) leads to a reduction of the stall phenomenon (vortex separation from the airfoil surface) (Ge et al., 2016; Paraschivoiu, 2002). However, it is necessary to use complex and expensive mechanisms to change the angle of attack. The increase in Reynolds number is also dependent on environmental conditions (Bogateanu et al., 2014). Optimizing the airfoil geometry and its parameters, which researchers commonly use, is considered the least expensive way to control the stall and improve the vertical axis wind turbine performance. Airfoils in the vertical axis wind turbine (VAWT) are usually selected from NACA 4-digit airfoils. Figure 1 illustrates the geometric parameters of a NACA symmetrical airfoil. The tip of the airfoil is the first part

Nomenclature

A	swept area	CFD	Computational Fluid Dynamics
C	class functions	CST	the class functions/shape functions transformation
C_p	power coefficient	FVM	Finite Volume Method
C_m	torque coefficient	LER	Leading-Edge Radius
N1,N2	airfoil constants	RANS	Reynolds-Averaged Navier–Stokes
$\bar{P}$	mean pressure	TSR (λ)	Tip Speed Ratio
p	power	VAWT	Vertical Axis Wind Turbine
S	shape functions	ω	Rotational speed
T	torque	ϑ	kinematic viscosity
U_∞	the free stream wind speed	θ	The angular position
$\overline{u_i}$	the average velocity	ρ	density
AOA	Angle Of Attack	τ_{ij}	Reynold's stress tensor

encountering the oncoming flow. Therefore, it significantly affects the flowing fluid. This parameter affects the intensity and quantity of vortices, making the turbine performance away from the ideal state (Wang & Zhao, 2016).

After developing the computational fluid dynamics, numerous researchers optimized the performance of the vertical axis wind turbine using this method (Meana-Fernández et al., 2018; Elsakka et al., 2022).

Meana-Fernández et al. (2018) examined the blade geometry parameter, the solidity of the turbine, and the Reynolds number of flow in a vertical axis wind turbine. Their evaluations of the geometric characteristics of a NACA 4-digit airfoil indicated that the impact of the geometric parameters, including the thickness and the maximum camber position of the airfoil in the Darrieus vertical axis wind turbine was more than other parameters.

Carrigan et al. (2012) optimized the overall airfoil in a vertical-axis wind turbine using a classification algorithm. In this study, the optimal solidity and thickness were calculated for NACA 0015 airfoil. It was determined that the vertical axis wind turbine with 0.88 solidity and 58% more thickness, as well as the maximum camber of 0.237, represented the highest efficiency. This is an inappropriate method (optimization using computer algorithms) to study the parametric airfoil geometry.

Nejat et al. (2017) applied the class function/shape function transformation (CST) technique (introduced by Kulfan (2007)) to optimize the airfoil parameters in a horizontal axis wind turbine and achieved an increase of 6% in turbine power by optimizing wind blade chord and twist angle using the CST method.

Carrigan et al. (2012) did not use CST geometric functions, and Nejat et al. (2017) studied horizontal-axis wind turbines in their work. No study were found regarding the effect of the leading-edge radius on the performance of the vertical-axis wind turbine. However, the leading-edge radius affects the vortex formation and the intensity of the vortices generated (Wang & Zhao, 2016); therefore, it has been effective on the dynamic stall of the turbine (one of the factors reducing the performance of the vertical axis wind turbine). This study evaluated the possibility of improving the turbine's performance

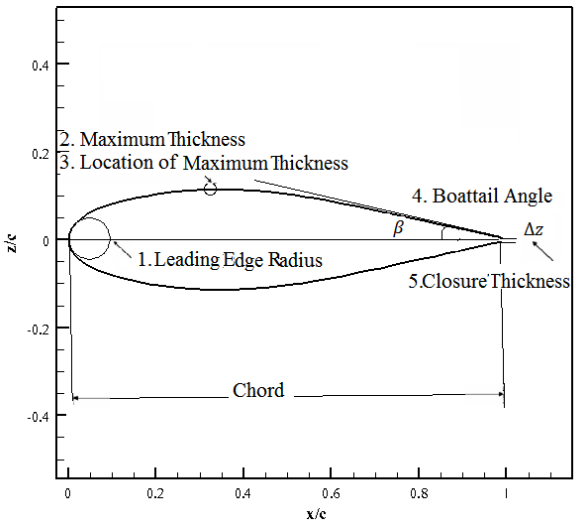

Fig. 1. Various parameters of four-digit series NACA symmetrical airfoil.

according to the importance of the effect of the airfoil geometry on the vertical axis wind turbine and the effect of the leading-edge radius on the fluid flow and dynamic stall of the vertical axis wind turbine.

2. METHODOLOGY

A Darrieus type straight blade vertical axis wind turbine with symmetrical blades, which is under the stall conditions in its Operating range (range of tip speed ratios) and hence, its performance has reduced due to the effect of this phenomenon, was selected in this study based on the experiment by Castelli et al. (2011) (Tables 1 and 2) Then, the turbine airfoil blade profile was changed using the CST method. In the first case, the leading-edge radius was increased by 10% to 30% in each step; however, in the second case, the leading-edge radius decreased by 10% to 30% in each step. Therefore, according to Table 3, blades with the leading-edge radius of 70, 80, and 90% of the primary leading-edge radius were generated in the case of the decreased leading-edge radius, and blades with the leading-edge radius of 110, 120, and 130% of the primary leading-edge radius generated in the case of the increased leading-edge radius. In the next step, the flow around the blades was simulated for geometries different from the

Table 1 Validation model main features

Turbine specifications	Quantity
Blade profile	NACA 0021
Blade chord (c)[mm]	85.8
R_{rotor}[mm]	1030
H_{rotor}[mm]	1456.4
$A_s[m^2]$	1.236
σ	0.5
Number of blades (N)	3
$H_{wind\ tunnel}$[mm]	4000
$w_{wind\ tunnel}$[mm]	3800
tested in Bovisa's low turbulence facility (Milan).	

Table 2 Flow specification in validation

Conditions	Measurement technique
$Re=3\times 10^5$	Low speed wind tunnel with an open, rectangular test
$U_\infty = 9$ m/s	

Table 3 specifications of different geometry

LER7	LER8	LER9	LER11	LER12	LER13
0%	0%	0%	0%	0%	0%

leading-edge radius using computational fluid dynamics and fluent software. Finally, the effects of the transient dynamics of the turbine on the fluid and overall performance of the turbine were examined by simultaneously comparing the contours for the flow and dimensionless coefficients of the performance, and accordingly, the optimized airfoil blade (NACA 0021) was introduced.

Kulfan (2007). introduced functions to estimate the airfoil geometry. He indicated that these functions represented various parameters of the airfoil and illustrated the airfoil's physical characteristics. According to the role of shape functions (S) and class functions (C) in creating diverse geometries of the airfoil blade, its method is CST. In this method, class and shape functions are used to determine the airfoil blade geometry. The expressions of the class function indicate the general shape of the geometry, and the expressions of the shape function represent (and control) the details of the geometry, such as the leading-edge radius, trailing-edge angle, and trailing-edge thickness (Ivanov et al., 2017) The CST method is defined as follows:

$$\frac{z}{c} = \boldsymbol{c}\left(\frac{x}{c}\right)\boldsymbol{s}\left(\frac{x}{c}\right) + \frac{x}{c}\frac{\Delta z}{c} \tag{1}$$

Where the class and shape function values are calculated by Equations 2 and 3.

$$\boldsymbol{c}\left(\frac{x}{c}\right) = \left(\frac{x}{c}\right)^{\boldsymbol{N1}}\left(\boldsymbol{1}-\frac{x}{c}\right)^{\boldsymbol{N2}} \tag{2}$$

$$\boldsymbol{s}\left(\frac{x}{c}\right) = \sum_{i=0}^{N}\left(A_i \frac{N!}{i!(N-i)!}\left(\boldsymbol{1}-\frac{x}{c}\right)^{N\_i}\right)\left(\frac{x}{c}\right)^{i} \tag{3}$$

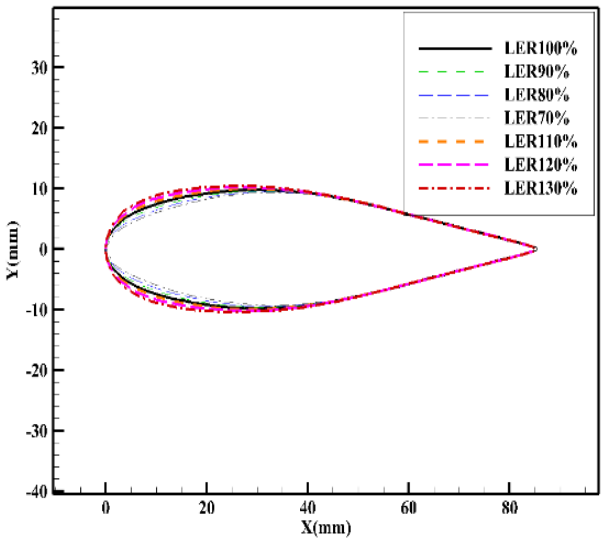

Fig. 2. Different geometric profiles created by CST method (Using the 4th order Bernstein function).

The constants N1 and N2 are determined based on the airfoil type. For the NACA-type round-nose airfoil, these values are 0.5 and 1, respectively.

$$\boldsymbol{s(0)} = \sqrt{\boldsymbol{2R_{LE}/c}} \tag{4}$$

$$\boldsymbol{s(1)} = \boldsymbol{tan\beta} + \boldsymbol{\Delta z/c} \tag{5}$$

It can be illustrated that the values of the leading-edge radius and the trailing-edge thickness are dependent on the value of the shape function (Kulfan, 2007; Ceze et al., 2009; Lane & Marshall, 2010).

In the CST method, the specific coefficients of the shape function (polynomial representing the specific geometry) should be calculated specifically. The Bernstein polynomial was used to calculate the unknown coefficients of the airfoil shape function. Figure 2 depicts the schematic of the leading-edge radius change.

3. NUMERICAL MODEL

3.1 Important Parameters

The flow velocity is denoted using the TSR ratio or λ in a wind tunnel laboratory. The speed ratio is a dimensionless quantity representing the ratio between the blade rotational speed and the free flow speed.

$$\boldsymbol{TSR} = \boldsymbol{R\omega / U_\infty} \tag{6}$$

In the above equation, ω denotes the rotational speed of the rotor, θ is the angular position of the blade rotation, and U_∞ represents the free stream wind speed.

Using the dimensionless coefficients of power, C_p and torque, C_m is a useful way to report the performance of the turbine. The comparison of the wind turbines performance is generally conducted using the power coefficient. This parameter is obtained by dividing the energy of the turbine by the total energy in the wind.

$$\boldsymbol{C_m} = \frac{\boldsymbol{T}}{\boldsymbol{1/2\rho A U_\infty{}^2 R}} \tag{7}$$

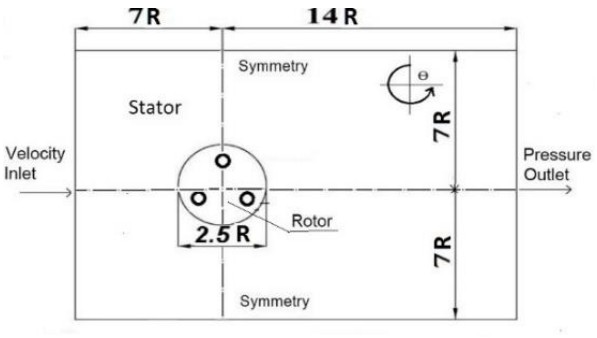

Fig. 3. Computational domain and boundary conditions.

$$C_p = \frac{T}{1/2\rho A U_\infty{}^3} \quad (8)$$

In the above equations, T is the toque, p denotes the power, ρ is the density of air, and A is the swept area of the vertical axis wind turbine.

3.2 Numerical Simulation Using the Computational Fluid Dynamics

Unsteady Reynolds-averaged Navier-stokes (URANS) equations were used in this research to numerically solve the incompressible viscous flow around the airfoil blades of turbines. These equations have been fully explained by a variety of researchers. For more detail, see (Sagharichi et al., 2017; Toudarbari et al., 2021).

The computational fluid dynamics and the ANSYS Fluent 18.2 software were applied in the fluid flow analysis, which uses the finite volume method (FVM) to discretize the equations. In this method, the unsteady and turbulent flow around the vertical axis wind turbine is simulated using Unsteady Reynolds-averaged Navier-stokes (URANS) equations and the turbulence model. The simulation performed in this study uses the k- ω SST turbulence model to analyze the flow disturbances. The sliding mesh method was used to simulate the turbine airfoil blade motions. In this method, the external area is assumed to be constant and the rotor area rotates with a given angular velocity corresponding to a 0.5-degree increment in each time step. (Smaller time steps have negligible effects on the accuracy). The second-order upwind scheme and the second-order implicit scheme were used to discretize the transfer equation and the terms of the equation of time, respectively. Eventually, the coupled analysis of the velocity-pressure discretized equations was conducted using the piezo algorithm.

3.2.1 Computational Domain

A two-dimensional plane perpendicular to the axis of the turbine and with dimensions larger than an actual wind tunnel was selected as the computational domain. According to the rotation of the airfoil blades using the sliding mesh method, this domain was divided into several smaller areas (sub-grids), including the rotor, airfoil blades, and stator. The moving area comprises three blades and a moving rotor surrounding the areas of the blades. The fixed area is a 21 × 14 rectangular to which the

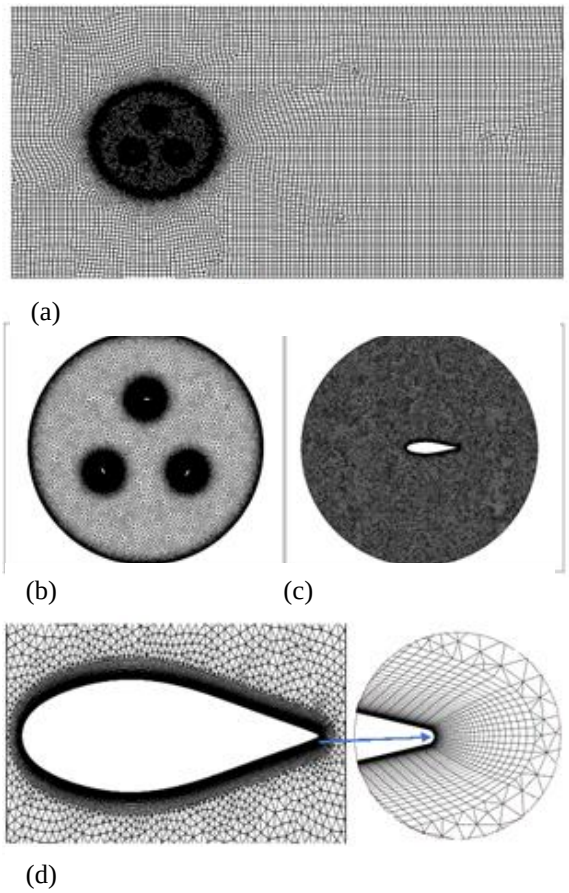

Fig. 4. Grid generation around wind turbine. (a): Computational domain, (b): Rotor area, (c): Mesh close to airfoil surface, (d): Airfoil boundary layer grids.

computational domain is limited. According to Fig. 3, the velocity inlet boundary condition at a speed of 9 m/s and the constant pressure condition (atmospheric pressure) were applied in the inlet face and outlet face, respectively. Owing to the infinite extent of the fluid around the blades and according to the physics of the problem, the shear stress in the upper and lower faces is zero. Therefore, the symmetry boundary condition used in this area represented the absence of shear stress in the upper and lower faces. Finally, the no-slip boundary condition was used in the face between the fluid and turbine airfoil blades.

3.2.2 Mesh Independence and Validation

A triangle and unstructured mesh was used to mesh the moving areas, and the fixed domain mesh is quadric and unstructured. Figure 4 presents a view of meshing the various areas of the domain. The highest density of meshing was used around the airfoil blades. Owing to the strong stress gradients, this area (the face between the fluid and the airfoil) was meshed using 45 rows of structured boundary layer mesh with a growth factor of 1.1 and high density. The skewness was always less than 0.8, and orthogonal quality was slightly more than 0.2 to maintain the quality of areas meshing. The value of y+ was also less than one in all calculations.

Furthermore, ensuring the independence of the numerical solution from the computational cell size and balancing the computational costs and the accuracy of the

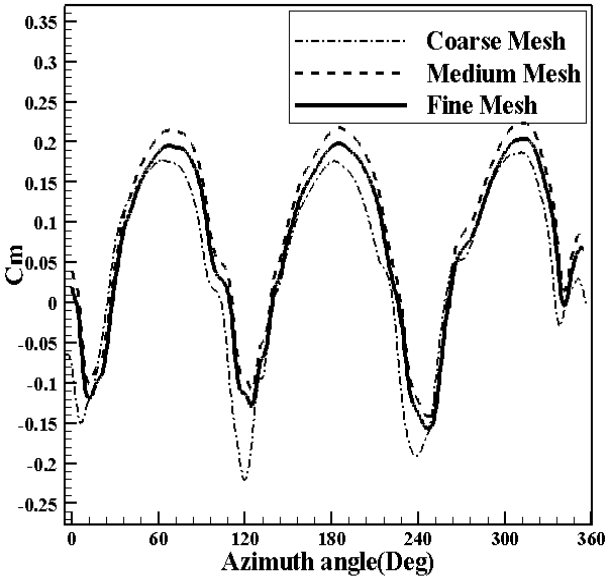

Fig. 5. Grid independency for simulation at TSR 2.

Table 4 The grid resolution details along the NACA0021airfoil

Grid	Number of Cells (Stator, Rotor, Airfoil)
Coarse	122000-29200-37000
Medium	132000-47000-88000
Fine	132000-86000-210000

calculations are significant to have an appropriate mesh. Figure 5 depicts the curve of the torque coefficient changes based on the azimuth angle changes for three types of different mesh (fine, medium, and coarse mesh).

Table 4 presents the number of computational cells related to each of these meshes separately sorted by the computational domain. According to Fig. 3, there are fewer differences between the values of the torque coefficient in the fine and medium mesh compared to that of the coarse and fine mesh. Considering the small difference between the values in the medium and fine mesh, this mesh was used to conduct other investigations of this research.

In the present study, the performance of a small Darrieus type straight blade vertical axis wind turbine with NACA 0021 airfoil blades was compared to the experimental results obtained by Castelli et al. (2011) using two-dimensional simulation and dimensionless parameters. Figure 6 provides the comparison of the curve related to the results of the numerical solution (using the k-ω SST turbulence model) to the experimental data reported by Castelli et al. (2011). Simplification of assumptions of two-dimensional simulation, including neglecting 3D effects of the flow and mechanical drop effect like not applying the blade rod caused the 2D simulation to be somewhat more than the experimental results.

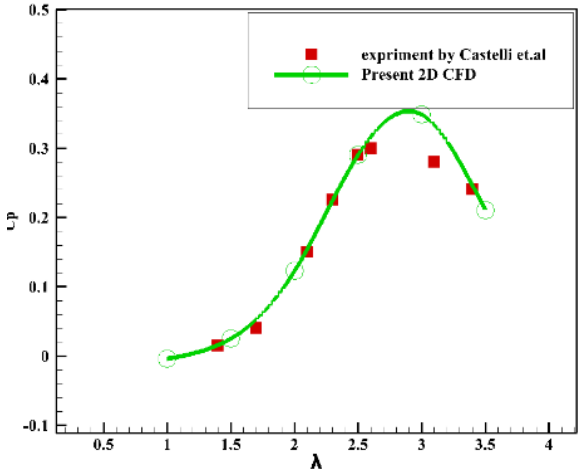

Fig. 6. Comparison of numerical results and experimental data.

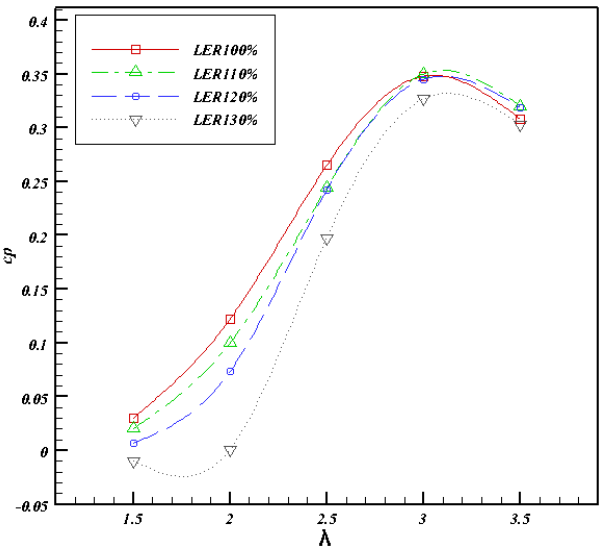

Fig. 7. Power factor curve in terms of tip speed ratio for increasing values of blade leading edge radius.

4. DISCUSSION

4.1 Vertical Axis Wind Turbine Performance Under the Effect of the Leading-Edge Radius

The performance of a vertical-axis wind turbine depends on several factors. The geometry effect, especially the geometric parameter of LER, on the dimensionless performance coefficient was examined in this section. This section presents the results of the 2D simulation of the vertical axis wind turbine with the aim of studying the effect of the leading-edge radius geometric parameter on the turbine performance. The power coefficient-tip speed ratio curve related to 6 different ratios of LER (LER70%, LER80%, LER 90%, LER110%, LER120%, and LER130%), which was developed in the previous stages, was evaluated to assess the role of LER. Figures 7 and 8 indicate the effect of LER on the power coefficient of the turbine. Figure 7 depicts the power

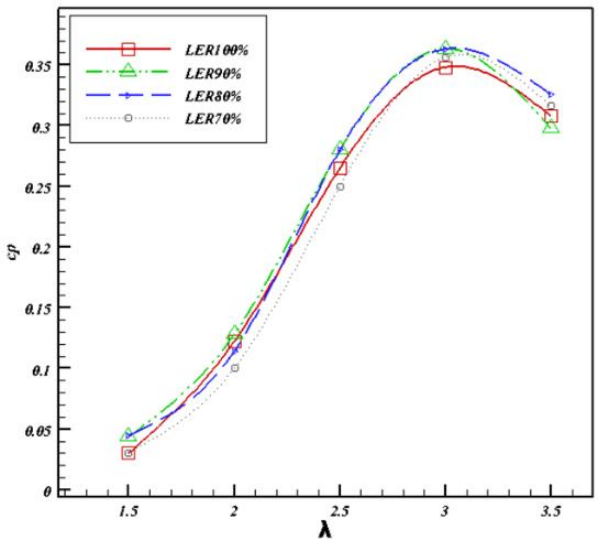

Fig. 8. Power factor curve in terms of tip speed for reduced values of blade leading edge radius.

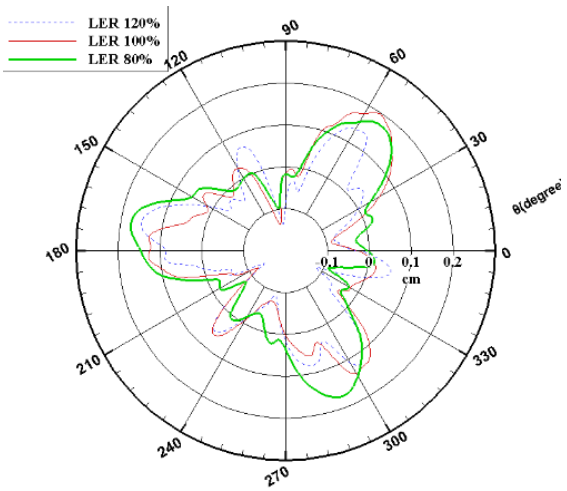

Fig. 9. Comparison of the torque coefficient for the Darius turbine with a variable radius at a tip speed of 1.5.

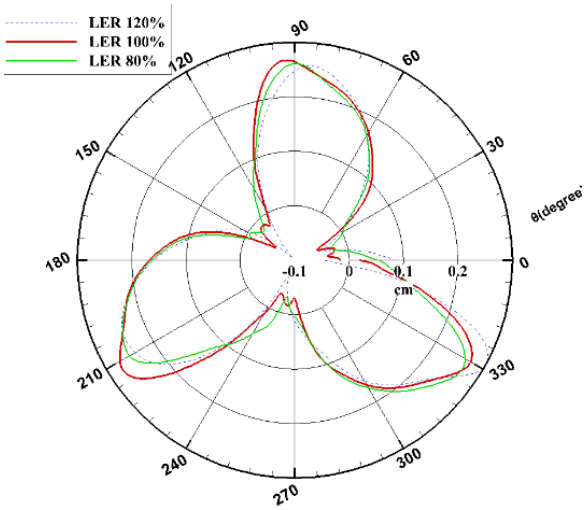

Fig. 10. Comparison of the torque coefficient for the Darius turbine with a variable radius at a tip speed of 2.

coefficient curve associated with the increasing ratios of LER and the primary airfoil (LER100%, LER110%, LER120%, and LER130%). According to Fig. 7, in a tip speed ratio lower than 3, the increased leading-edge radius reduces the power coefficient at a constant speed, so each step of increasing the leading-edge radius has intensified the reduction in the coefficients. Airfoil blades with a larger radius generate more drag when they encounter incoming fluid. This force plays an undesired role in the maximum efficiency of the turbine. The effect of the drag term is reinforced at a tip speed ratio greater than 3, and the power coefficient curve illustrates a downward trend (Jahanmiri et al., 2016).Within this range, power coefficients are reduced under the influence of a reduction in the lift-to-drag ratio, and the maximum performance value decreases quickly. Figure 8 depicts the curve of the power coefficients associated with the reduced ratios of LER and the primary airfoil (LER100%, LER90%, LER80%, and LER70%). According to this figure, the decreasing values of LER improved the optimum performance of the vertical axis wind turbine. The optimum power coefficients in turbines with LER80% and LER90% blades are approximately 7% higher than that in the turbine equipped with the primary airfoil. These blades also improved the power coefficient at a tip speed ratio of 1.5 by approximately 50%, and accordingly, they reinforced the turbine's self-starting capability.

Figure 9 and 10 present a comparison of the resulting diagram of the blades' torque coefficient-rotation angle for several different geometries of LER (LER80%, LER100%, and LER120%) at the tip speed ratios of 1.5 and 2.5. In both cases, the maximum output torque was extracted in the first half cycle of the turbine rotation. In this part of the turbine, the passing flow has a velocity higher than that of the other area; and since the power is proportional to the speed cubed, the maximum power available to the airflow is in this area.

As Fig. 9 shows, the use of a decreasing leading-edge radius increased the torque of the turbine in the second half cycle of the rotation and reduced the amount of generating negative torque in this area. This resulted in the improved performance of the turbine. By comparing Fig. 9 and 10, it can be concluded that the effect of the decreased leading-edge radius was more at a tip speed ratio of 1.5. The stall phenomenon significantly affects the turbine performance at this speed (Mohamed et al., 2015). As mentioned, LER is effective in controlling the flow separation and vortices that have the opportunity to separate from the airfoil blade at a high angle of attack with sharp changes and angles higher than the static stall limit; these are the reasons to develop the dynamic stall in the vertical axis wind turbine. Since the dynamic stall of the turbine was the reason for reducing the torque and lift of the turbine at this tip speed ratio, the reduction of the leading-edge radius improved these conditions and increased the produced torque.

In Fig. 11, the curve of the torque produced by the blade based on the rotation angle at different tip speed ratios ($1.5 < \lambda < 3$) for turbines equipped with the reduced leading-edge radius (LER80%, LER90%) is compared to that of the torque produced by the blade in the primary state. According to the produced torque curve, the effect

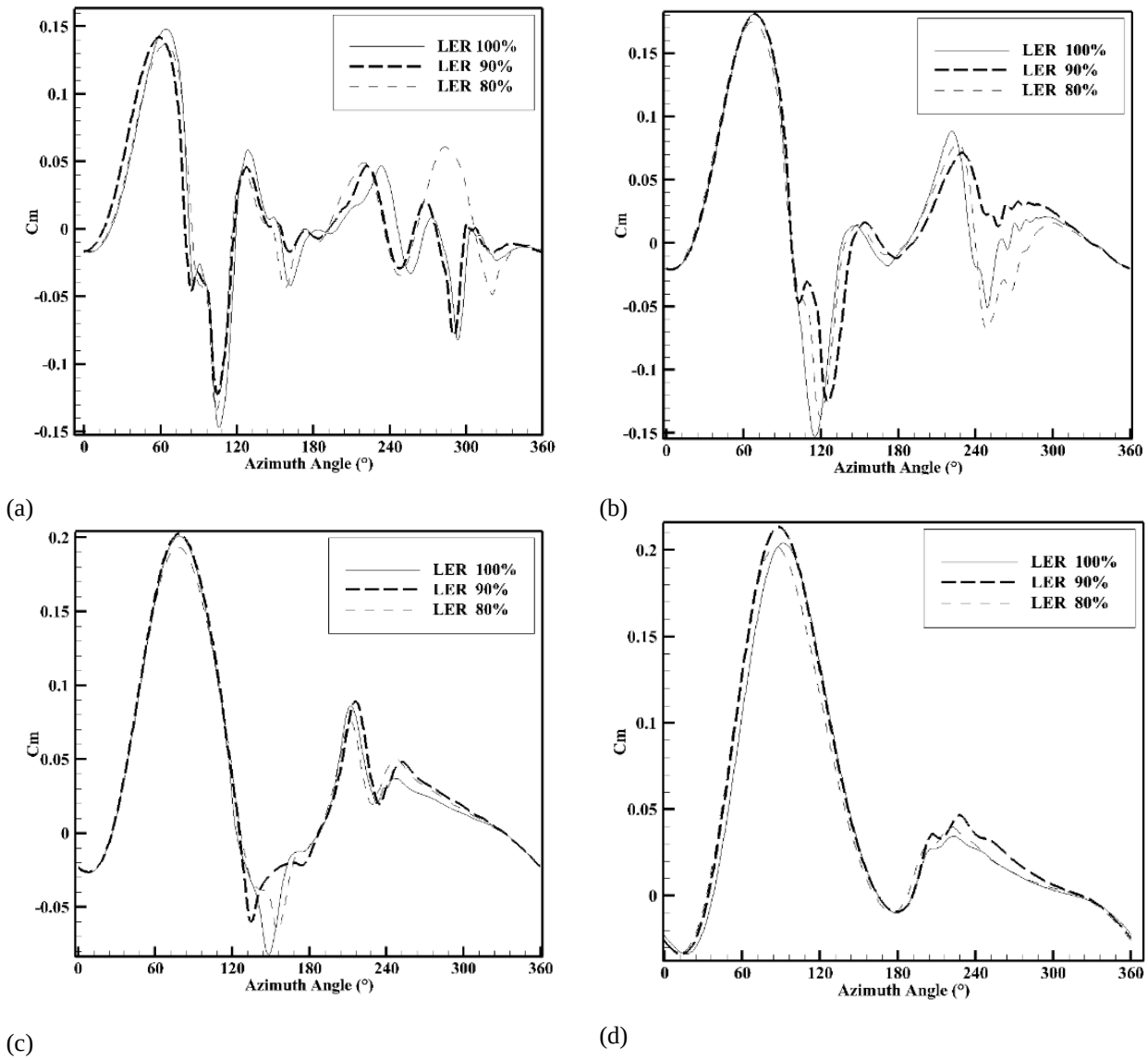

Fig. 11. torque produced by reduced leading edge radius blade at different tip speed (a): 1.5, (b): 2, (c): 2.5, (d): 3.

of reducing the leading-edge radius on improving the produced torque is higher at low-tip speed ratios.

According to Fig. 11(a), most fluctuations of the torque curve occurred at λ=1.5. The existence of a greater range of changes in the torque-angle curve for an airfoil blade with LER100% than other blades is considered a factor to intensify the fatigue phenomenon in the vertical axis wind turbine at this LER ratio. As the figure shows, the airfoil blade with LER80% reduced the range of torque fluctuations under equal conditions and at λ=1.5. In addition, the airfoil blade with LER80% produced more torque at λ=1.5 than airfoil blades with LER90% and LER100%. The airfoil blade with LER90% improved the produced torque at tip speed ratios of 1.5, 2, and 2.5, and in the range under discussion, it reduced the production of negative torque.

According to Fig. 11 (c), the effect of the reduced LER on improving the torque was reduced by decreasing the effects of the stall phenomenon at a tip speed ratio of 2.5. However, as Fig. 11(c) and 11(d) display, LER80% and LER90% also improved the production of torque at higher speed ratios. This improvement occurred due to the leading-edge radius effect in encountering the fluid flow and reducing the drag. In the following, the effects of the leading-edge radius on the fluid flow are evaluated.

4.2 Effects of the Leading-Edge Radius on the Fluid Flow

The evaluation of the produced torque-azimuth angle curve at a tip speed ratio of less than 2 indicated that the turbine performance turned away from its ideal state under the influence of aerodynamic effects like the stall. Hence, the performance coefficients are considerably reduced during the airfoil motion, especially in the second half cycle of rotation. It was also found that the airfoil blade with the decreased radius improved the produced torque at a low-tip speed ratio (1.5). The effect of the leading-edge radius on aerodynamic phenomena and generally on the passing fluid flow was examined using the vorticity contour for the flow in this section.

Figures 12 to 15 illustrate the vorticity of turbines with LER110%, LER100%, and LER90% with 90-degree

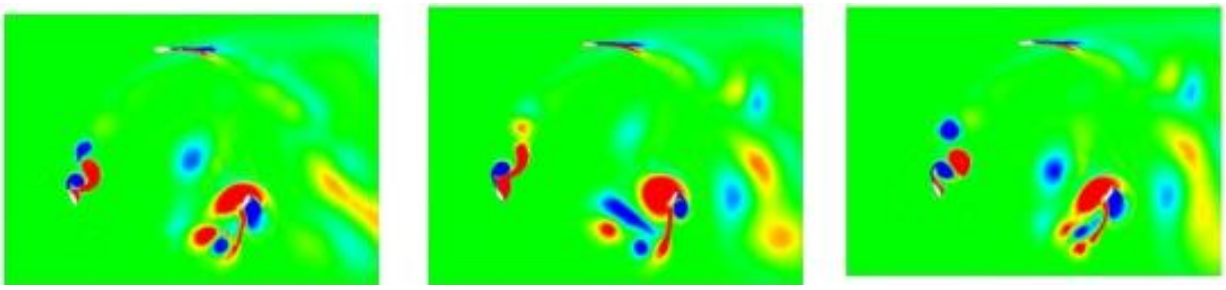

(a) (b) (c)

Fig. 12. Vorticity contour of blade at 0 ° (a): LER110, (b): LER100, (c): LER90 at TSR 1.5.

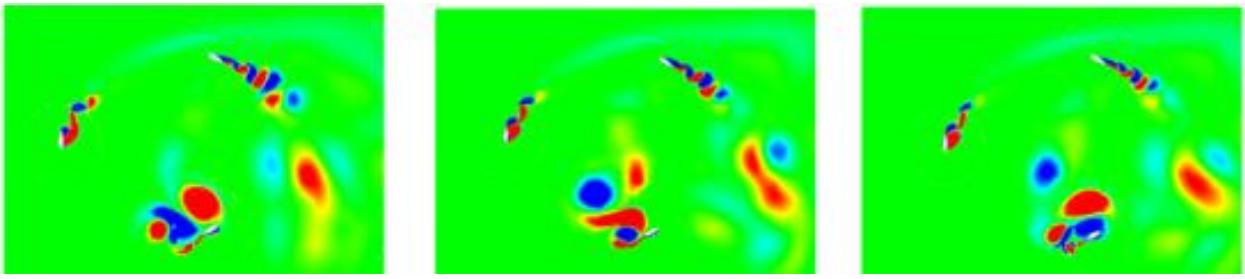

(a) (b) (c)

Fig. 13. Vorticity contour of blade at 90 ° (a): LER110, (b): LER100, (c): LER00 at TSR 1.5

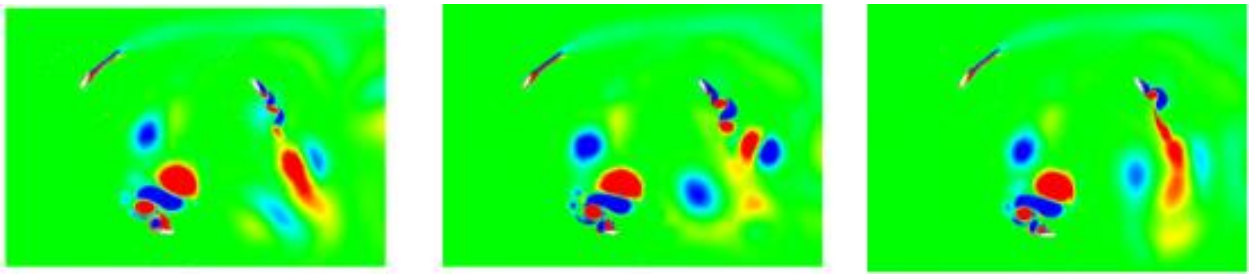

(a) (b) (c)

Fig. 14. Vorticity contour of blade at 180 ° (a): LER110, (b): LER100, (c): LER90 at TSR 1.5

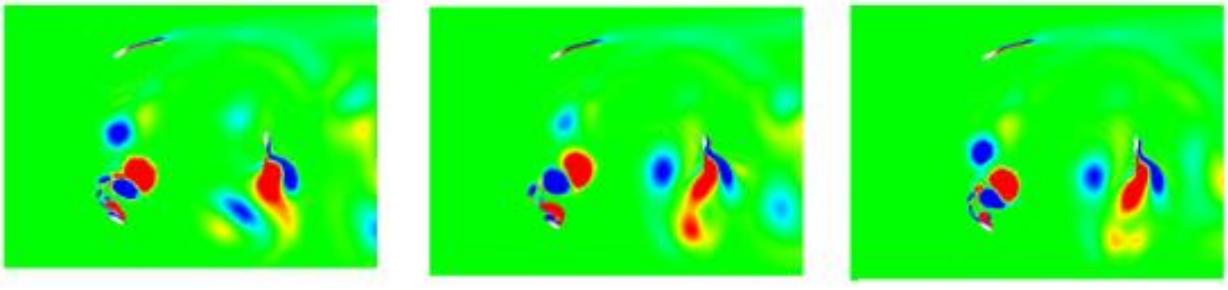

(a) (b) (c)

Fig. 15. Vorticity contour of blade at 270 ° (a): LER110, (b): LER100, (c): LER90 at TSR 1.5

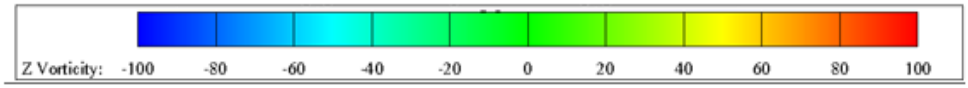

phase shift at a tip speed ratio 0f 1.5 after stationary steady conditions are met. Figure 12 indicates the initial position of the motion. In this case, the first blade is at the 0-degree rotation angle and the second and third blades are placed at 120 and 240 degrees, respectively. At the beginning of the rotation (at 0 degrees), no vortex is formed around the first blade due to the low angle of attack. As the first blade passes through the angle of 90 degrees and a little after that, vortices are formed around this blade in the first half cycle of rotation. Considering the Vorticity field around the turbine blade with LER110% at 90 degrees, it can be concluded that the strength of the vortices around this blade at this ratio of LER is higher than LER100% and LER90%. The increased intensity and quantity of the vortices around the blade with LER110% in the first half cycle of rotation and at a 180-degree angle can also be

observed around the first blade. However, the vortex around the blade with LER90% at the same angles is smaller than that in other states. It is clear that smaller vortices damp faster and reduce the probability of collisions with blade in the downstream. Figures 14(c) and 15(c)show that reduced leading-edge radius initially improves near wake in the first half cycle of rotation than empowering the airfoil to have less vortex shedding and stall in the second half cycle of rotation. On the other hand, according to Fig. 14(a, b) and 15(a, b) increasing the leading-edge radius adversely affect the flow quality around the blades by creating more strong vortices and strengthening the turbulent intensity of the flow. A turbine with LER110% increased the turbulent intensity of the flow; however, the turbine with LER90% reduced this intensity. Indeed, the most significant effect of the reduced LER in the first half cycle of rotation is the reduction of the turbulent intensity and the flow separation effects by controlling the vortices. Given that most of the vortices are formed in this part of the turbine, the use of a decreasing LER is highly useful in controlling the dynamic stall.

4.3 Performance Improvement Based on Leading-Edge Radius Change

The optimization of the leading-edge radius with two mechanisms of controlling the dynamic stall and reducing the drag at a tip speed ratio of $1 < \lambda < 3.5$ improves the performance of the vertical axis wind turbine. The starting characteristics of lift-type VAWT were already introduced as one of its problems. When the blades start to move (at a low-tip speed ratio), the initial performance of the turbine encounters a problem. The blades do not have enough momentum to continue their motion at this point, and the turbine has negative performance due to the flow separation and the formation of vortices. This state, also called the dead zone, means that at the beginning of its movement, the turbine does not have enough power to pass through this critical region and reach its optimal performance conditions. According to Fig. 7, the LER optimization effectively improved the power coefficient at a speed ratio of 1.5 and applying the profile of LER80% and LER90% increased the power coefficient of the turbine at this speed ratio by almost 50%. In addition to strengthening the self-starting of the turbine, the power coefficient improves the performance in the studied domain and increases the optimum performance of the vertical axis wind turbine (approximately 7%). Another benefit of optimizing leading-edge radius is to improve the performance in the operating range of the turbine. The power coefficient of the turbine equipped with a standard blade quickly leaves the optimal performance zone under the impact of the drag term when the tip speed ratio exceeds a specified limit ($\lambda > 3$). As the optimum operating range of the turbine becomes wider, there is a greater possibility for the turbine to operate in this area and extract greater torque. Hence, the use of LER80% increases this range, and its application for special design aiming at improving this range is appropriate. Researchers considered turbine fatigue and vibrations as another issue during optimization (Mabrouk et al., 2017; Castellani et al., 2019). In the optimal radius mode, the airfoils are far less placed in areas with negative torque due to better separation control than in the initial state. Therefore, using LER80% and LER90% effectively reduces the vibrations and dead band region of VAWT. Table 5 summarizes the effects of leading-edge radius on turbine performance. Based on this table, both a 10% and 20% decrease in leading-edge radius improves the performance of the turbine.

Table 5 Performance improvement base on the leading-edge radius

	Negative torque production	**Optimum oprating performance**	**Vibration**	**Operating range**
LER 80%	Reduced	7% Improvement	Reduced	Unchanged
LER 90%	Reduced	7% Improvement	Reduced	Increased

5. CONCLUSION

In this study, the effect of leading-edge radius on the performance of Darrieus vertical axis wind turbine was numerically evaluated. ANSYS Fluent software, with k-ω SST turbulence model were used in all simulations. The results demonstrate that:

1- By reducing the ratios of leading-edge radius increase the torque production in the second half cycle of the rotation is increased. This improves the blade performance during the rotation. The improvement occurs owing to the effect of LER on dynamic stall.

2- The reduced LER is highly effective in reducing the fluctuations of the turbine at low-speed ratios through the control mechanism of the vortex separation. The effect of LER on the produced torque of turbine is gradually reduced by increasing the speed ratio and decreasing the angle of attack.

3- The optimal LER mode reduces the negative torque of the turbine and, as a consequence, reduces the dead band region.

CONFLICT OF INTERESTS

The authors have no conflict of interests to disclose.

AUTHORS CONTRIBUTION

N. Davandeh: conceptualization, data-curation, formal-analysis, funding-acquisition, investigation, methodology, resources, software, validation, visualization, writing-original-draft, writing-review-editing; M. J. Maghrebi: formal-analysis, funding-acquisition, methodology, project-administration, resources , supervision , writing-review-editing.

REFERENCES

Bogateanu, R., Dumitrache, A., Dumitrescu, H., & Stoica, C. I. (2014). Reynolds number Reynolds number effects on the aerodynamic performance of small

VAWTs. *UPB Scientific Bulletin, Series D: Mechanical Engineering*, 76(1), 25-36.

Carrigan, T. J., Dennis, B. H., Han, Z. X., & Wang, B. P. (2012). Aerodynamic shape optimization of a vertical-axis wind turbine using differential evolution. *ISRN Renewable Energy*, 2012. https://doi.org/10.5402/2012/528418

Castellani, F., Astolfi, D., Peppoloni, M., Natili, F., Buttà, D., & Hirschl, A. J. M. (2019). Experimental vibration analysis of a small scale vertical wind energy system for residential use. Machines, 7(2), 35. https://doi.org/10.3390/machines7020035

Castelli, M. R., Englaro, A., & Benini, E. J. E. (2011). The Darrieus wind turbine: Proposal for a new performance prediction model based on CFD. Energy, 36(8), 4919-4934. https://doi.org/10.1016/j.energy.2011.05.036

Elsakka, M. M., Ingham, D. B., Ma, L., Pourkashanian, M., Moustafa, G. H., & Elhenawy, Y. (2022). Response surface optimisation of vertical axis wind turbine at low wind speeds. *Energy Reports*, 8, 10868-10880. https://doi.org/10.1016/j.egyr.2022.08.222

Ge, M., Tian, D., & Deng, Y. (2016). Reynolds number effect on the optimization of a wind turbine blade for maximum aerodynamic efficiency. *Journal of Energy Engineering*, 142(1), 04014056. https://doi.org/10.1061/(ASCE)EY.1943-7897.0000254

Ivanov, T. D., Simonović, A. M., Svorcan, J. S., & Peković, O. M. (2017). VAWT optimization using genetic algorithm and CST airfoil parameterization. FME Transactions, 45(1), 26-31. https://doi.org/10.5937/fmet1701026I

Jahanmiri, M., Shooshtaryrezvany, A., & Nirooei, M (2016). A computational study of the effect of blade thickness on performance of vertical axis wind turbine. IOSR Journal of Mechanical and Civil Engineering, 13(5), 57-65. https://doi.org/.10.9790/1684-1305025765

Karbasian, H. R., Esfahani, J. A., Aliyu, A. M., & Kim, K. C. (2022). Numerical analysis of wind turbines blade in deep dynamic stall. *Renewable Energy*, 197, 1094-1105. https://doi.org/10.1016/j.renene.2022.07.115

Kulfan, B. M. (2007). The "CST" universal parametric geometry representation method, Recent Extensions and Applications. In *Proc R Aeronaut Soc Conf* (Vol. 114, No. 1135, pp. 157-176).

Lane, K., & Marshall, D. (2010*). Inverse airfoil design utilizing CST parameterization*. 48th AIAA Aerospace Sciences Meeting Including the New Horizons Forum and Aerospace Exposition.

Lee, S. M., & Jang, C. M. (2016). *performance evaluation of a small darius wind turbine installed at duckjeok island in korea.* Fluids Engineering Division Summer Meeting. (Vol. 50299, p. V01BT29A006). American Society of Mechanical Engineers. https://doi.org/10.1115/FEDSM2016-7818

Mabrouk, I. B., El Hami, A., Walha, L., Zghal, B., Haddar, M. J., & Processing, S. (2017). Dynamic vibrations in wind energy systems: Application to vertical axis wind turbine. *Mechanical Systems and Signal Processing*, 85, 396-414. https://doi.org/10.1016/j.ymssp.2016.08.034

Meana-Fernández, A., Solís-Gallego, I., Oro, J. M. F., Díaz, K. M., & Velarde-Suárez, S. J. E. (2018). Parametrical evaluation of the aerodynamic performance of vertical axis wind turbines for the proposal of optimized designs. *Energy*, 147, 504-517. https://doi.org/10.1016/j.energy.2018.01.062

Mohamed, M., Ali, A., & Hafiz, A. A. (2015). Effect of blade cambering on dynamic stall in view of designing vertical axis turbines. *Journal of Fluids Engineering*, 140(6). https://doi.org/10.1115/1.4039235

Ouro, P., Stoesser, T., & Ramirez, L. (2018). Effect of blade cambering on dynamic stall in view of designing vertical axis turbines. *Journal of Fluids Engineering*, 140(6). https://doi.org/10.1115/1.4039235

Paraschivoiu, I. (2002). *Wind turbine design: with emphasis on Darrieus concept.* Presses inter Polytechnique.

Ragheb, M. (2008). Wind turbines in the urban environment. Retrieved July, 12, 2009.

Sagharichi, A., Maghrebi, M. J., & ArabGolarcheh, A. (2017). Numerical Investigation of the Effect of Fixed and Variable Pitch Angle Blade on Dynamic Stall of Flow Field Around Darrieus Wind Turbine Blade. *Fluid Mechanics & Aerodynamics Journal*, 5(1). 29-46.

Shahizare, B., Nik-Ghazali, N., Chong, W. T., Tabatabaeikia, S., Izadyar, N., & Esmaeilzadeh, A. (2016). Novel investigation of the different Omni-direction-guide-vane angles effects on the urban vertical axis wind turbine output power via three-dimensional numerical simulation. *Energy Conversion and Management*, 117, 206-217. https://doi.org/10.1016/j.enconman.2016.03.034

Taban, A., Jalali, A., & Zamani, M. (2020). Effect of blade angle of attack on the performance of the darius j-shaped vertical axial wind turbine. *Modares Mechanical Engineering*, 20(7), 1773-1788.

Toudarbari, S., Maghrebi, M. J., & Hashemzadeh, A. (2021). Evaluation of Darrieus wind turbine for different highway settings using CFD simulation. *Sustainable Energy Technologies and Assessments*, 45, 101077. https://doi.org/10.1016/j.seta.2021.101077

Wang, Q., & Zhao, Q. (2016). Experiments on unsteady vortex flowfield of typical rotor airfoils under dynamic stall conditions. *Chinese Journal of Aeronautics*, 29(2), 358-374. https://doi.org/10.1016/j.cja.2016.02.013